A Time-Lagged Ensemble Simulation on the Modulation of Precipitation over West Java in January–February 2007

NURJANNA J. TRILAKSONO,* SHIGENORI OTSUKA, AND SHIGEO YODEN

Department of Geophysics, Kyoto University, Kyoto, Japan

ABSTRACT

A numerical experiment using a regional nonhydrostatic model is performed to investigate the synoptic condition related to the heavy precipitation event that occurred at Jakarta in West Java, Indonesia, in January–February 2007. A time-lagged ensemble forecast method is employed with nine ensemble members. The ensemble mean well reproduces the temporal modulation of the spatial distributions of precipitation obtained from the Tropical Rainfall Measuring Mission data.

During the simulated two months, several monsoon surges are observed, but only the surge event during which the Jakarta flood event occurred is associated with a cold anomaly. The top of the cold northerly is about 1.5 km. The cold surge event is preceded by the so-called Borneo vortex event, which is dominated by a cyclonic vortex around Borneo, Indonesia, with a horizontal scale of 1000 km and a vertical scale of 3 km.

An analysis of cumulative distribution functions in a pentad time scale shows the modulation of the probability of rainfall rate. In pentad 7 (31 January–4 February), which includes the heavy rainfall event, the fraction of the area with precipitation is the highest and the contribution of heavy rainfall to the total amount is one of the highest in the two-month period. The diurnal cycle of occurrence of heavy rainfall is also modulated; in pentad 7, semidiurnal variation becomes dominant, and the largest peak appears in the early morning.

1. Introduction

Natural disasters related to severe weather events (e.g., flood and landslide caused by heavy rainfall) often occur in Indonesia and have great impacts on human life. The occurrence dates and places of such severe disasters and some numbers of losses and damages are presented in Table 1, which is taken from the Indonesian Disaster Data and Information (DiBi) database compiled by the National Disaster Management Agency (BNPB) of the Republic of Indonesia (available online at http://dibi.bnpb.go.id). Only events in which more than 45 people were killed are selected from the disasters that occurred in a 7-yr period during 2002–08. Among the nine selected events, the Jakarta (in West Java,

Indonesia) flood event in February 2007 was a devastating disaster and is considered the worst in the last three decades; 48 people were killed, 521 389 people were evacuated, and 24 957 houses were damaged.

The Jakarta flood event on February 2007 occurred mainly because of heavy rainfall for several times from 31 January to 2 February. According to the Indonesian Meteorological, Climatological, and Geophysical Agency (BMKG) report, the highest daily rainfall was 340 mm, which was measured on 2 February at Pondok Betung Station (6.2°S, 106.6°E). Torrential rains that repeatedly occurred over West Java coincided with a strong and persistent transequatorial monsoon surge from the Northern Hemisphere (Wu et al. 2007). The strong monsoon flow near the surface and the upper southeasterly wind over it produced a low-level vertical shear of winds. The shear with wet lower and dry middle layers allowed the severe moist convections to develop repeatedly.

Tangang et al. (2008) analyzed the extreme precipitation that resulted in floods in southern Peninsular Malaysia in mid- and late December 2006 and mid-January 2007, before the Jakarta flood event. They showed that

* Additional affiliation: Faculty of Earth Sciences and Technology, Institut Teknologi Bandung, Bandung, Indonesia.

Corresponding author address: Shigeo Yoden, Department of Geophysics, Kyoto University, Kyoto 606-8502, Japan.
E-mail: yoden@kugi.kyoto-u.ac.jp

TABLE 1. Numbers of affected people and damaged houses due to natural disasters associated with severe weather events in Indonesia for the period from 1 Jan 2002 to 31 Dec 2008. Data source from National Disaster Management Agency (BNPB) of the Republic of Indonesia. Asterisk refers to the 2007 Jakarta flood event.

Event	Date	Province	Killed	Injured	Evacuated	Damaged houses
Floods	2 Nov 2003	Sumatra Utara	160	50	2080	437
	1 Feb 2007*	DKI Jakarta	48	484	521 389	24 957
Floods and landslides	28 Jan 2003	Jawa Barat	59	74	1796	168
	1 Jan 2006	Jawa Timur	92	68	7644	397
	1 Jun 2006	Sulawesi Selatan	210	18	7858	972
	22 Jul 2007	Sulawesi Tengah	76	2371	17 078	240
	26 Dec 2007	Jawa Tengah	62	85	501	1590
Landslides	21 Feb 2005	Jawa Barat	137	—	315	80
	4 Jan 2006	Jawa Tengah	76	16	587	104

the extreme precipitation events were associated with the strong northeast cold surge that interacted with other synoptic systems such as the Madden–Julian oscillation (MJO) or the Borneo vortex (e.g., Cheang 1977). It is a cyclonic vortex with a horizontal scale of 1000 km around Borneo, Indonesia. In days without a Borneo vortex, deep convection tends to be suppressed over the South China Sea and Borneo and enhanced downstream over the landmasses on the western and southern peripheries of the equatorial South China Sea (Chang et al. 2005). The pattern is reversed in days with a vortex. Another example of a strong cold surge that had a role on heavy rainfall event in Thailand was reported by Wangwongchai et al. (2005) for the case study of 20–23 November 2000. In that case, the cold surge blew southwestward over the South China Sea, which turned into southeastward at 5°N, forming a cyclonic circulation over Malaysia and Sumatera. This circulation was associated with the maximum of the convergence of total moisture flux near South Thailand, which was favorable for the occurrence of the heavy rainfall.

During such strong surge events, stronger winds occur over East Asia and the South China Sea. In about 5 days after strong surge events over the South China Sea, cross-equatorial flows occur over the Indonesian region and the cross-equatorial flows thereafter influence the circulation pattern over Indonesia and northern Australia (Suppiah and Wu 1998). The extension of cold surges crossing the equator is primarily due to the strengthening of northeasterly near the surface. The flow is restricted by topography such that it is channeled toward the equator (Chang et al. 2005), and the layout of the Indonesian islands enables cold surges to reach Java. Cold surges are typically dry, but as they pass over the South China Sea, they get moistened (Johnson and Houze 1987). Such conditions are favorable for moist convections to develop.

Numerical study is a powerful approach to understand the characteristics of meteorologically interesting events; it reveals physical processes of the events in detail and it gives three-dimensional structures of the events and their time evolutions. Until now, however, only a few numerical studies addressed extreme precipitation events related to the monsoon in tropical Asia. One example is given by Juneng et al. (2007), who studied an extreme rainfall event during 9–11 December 2004 over the east coast of Peninsular Malaysia. Their study revealed an important role of local topography in providing the forcing for moist air lifting and another role of latent heat release crucial for supporting the vertical motion associated with the rainfall. Another example on the simulation of heavy rainfall system in tropical Asia was documented by Seko et al. (2008). An intense rainfall system that developed in Mumbai, India, on 26 July 2005 was successfully simulated with a multinesting system with horizontal resolutions of 20, 5, and 1 km without cumulus parameterization. Increase of the horizontal resolution was a key factor for the reproduction of heavy rainfall, because the local topography with steep gradients around Mumbai was important for the occurrence.

Mesoscale convective systems include random processes in space and time. Therefore, probabilistic information would be useful to study heavy rainfall events associated with mesoscale convective systems. As ensemble forecasting is a standard approach to obtain probabilistic information, it would be an alternative approach to utilize a given computer resource with a relatively coarse-resolution model with cumulus parameterizations to perform an ensemble simulation, even though heavy precipitation induced by local topography might be underestimated. Ensemble numerical weather prediction with a global model became a standard technique in the 1990s at operational weather forecast centers, while that with a regional mesoscale model is still an interesting and greatly challenging subject (e.g., Yoden 2007).

In the tropics, precipitation has large amplitudes in its diurnal cycle, which highly depends on geographical

location and local time (e.g., Mori et al. 2004; Hirose and Nakamura 2005). Because of the existence of spinup processes, ensemble simulations in the tropics may have biases on local precipitation if all the ensemble members are started from one initial time in a day. To avoid such a diurnal cycle problem in ensemble simulations, a time-lagged ensemble technique (Branković et al. 1990) is used in this study. A regional model that consists of a single domain with a relatively coarse resolution is used to perform ensemble simulations for the two-month period including the Jakarta flood event. Based on the ensemble simulation data, we investigate the temporal modulation of three-dimensional synoptic fields and precipitation in the periods before, during, and after the heavy rainfall in Jakarta in 2007. Key features of the synoptic field are cold surge, cross-equatorial flow near the surface, and the appearance of the Borneo vortex. We also investigate frequency distribution functions in pentad time scales to characterize the statistical feature of heavy rainfall. The paper is organized as follows. Section 2 explains the experimental design. Section 3 presents the results of the analysis of the ensemble simulation data. Section 4 provides a discussion and conclusions are drawn in section 5.

2. Experimental design

The numerical model used in this study is the Japan Meteorological Agency Nonhydrostatic Model (JMA-NHM; Saito et al. 2006, 2007). We set up a single computational domain with a 20-km horizontal resolution. The domain has 103×115 grid points centered at 5°S, 110°E and covers about 14°S–4°N, 100°–120°E on a Mercator projection. The topography of the domain is presented in Fig. 1. The model employs a terrain-following coordinate system with 40 layers and the top of the model is located at 22.1 km above the ground. The subgrid-scale parameterization schemes and parameter settings that we employed are basically the same as those of Hayashi et al. (2008) with their recommended values tuned for the 20-km horizontal resolution. The cumulus parameterization scheme is a modified Kain–Fritsch. The cloud microphysics scheme is a 6-class bulk microphysics. The GSM0412 radiation scheme (Yabu et al. 2005) and an improved Mellor–Yamada level 3 planetary boundary layer scheme (Nakanishi and Niino 2004, 2006) are used. The National Centers for Environmental Prediction (NCEP) Global Tropospheric Analyses (final analyses) with the horizontal resolution of $1° \times 1°$ and the time interval of 6 h are used for the model input.

To run the time-lagged ensemble simulation, we follow the same procedure and method used by Mittermaier
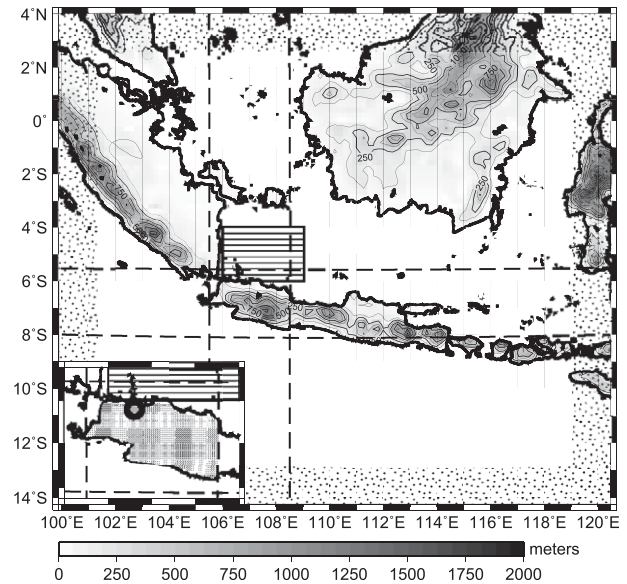

FIG. 1. The model domain of computation. Shading and contours show topography (m) of the domain. The two horizontal dashed lines denote the latitudes of 5.5° and 8°S. The zonal belt is used for cross-sectional analyses in Fig. 3. The two vertical dashed lines denote the longitudes of 105.5° and 108.5°E. The meridional belt is used for cross-sectional analyses in Figs. 4, 5, and 8. The dotted region near the side boundaries is not used in the analyses. The box with a horizontal hatch pattern that covers the area between 4°–6°S and 106°–109°E is used for Fig. 12. The inset map shows West Java. The circle in the inset map denotes the location of Pondok Betung Station. The hatched area in the inset map is used for Figs. 11 and 12.

(2007), but for the length of individual simulation (72 instead of 36 h). We perform 72-h simulations every 6 h, and exclude the initial 18 h from analyses to avoid the effect of unrealistic convections in the spinup processes. Thus, the number of ensemble members becomes nine. We analyze the 2-month period (12 pentads) from 0000 UTC 1 January to 2300 UTC 1 March 2007. The model output is sampled every 1 h.

To validate the numerical results, we use the Tropical Rainfall Measuring Mission (TRMM) 3B42 product (Huffman et al. 2007), which is estimated rainfall data for $0.25° \times 0.25°$ grid boxes in every 3 h. The TRMM data show the correlation coefficient of 0.56 with the rain gauge data at Soekarno-Hatta near Jakarta for the 2-month period. We also use the daily sea surface wind of the National Aeronautics and Space Administration (NASA) Quick Scatterometer (QuikSCAT) L3 (see online at http://podaac.jpl.nasa.gov/dataset/QSCAT_LEVEL_3) product, which provides gridded winds at 10 m above the sea surface with a spatial resolution of $0.25° \times 0.25°$ (e.g., Freilich and Dunbar 1999; Chelton and Freilich 2005), to validate the model-simulated surface winds.
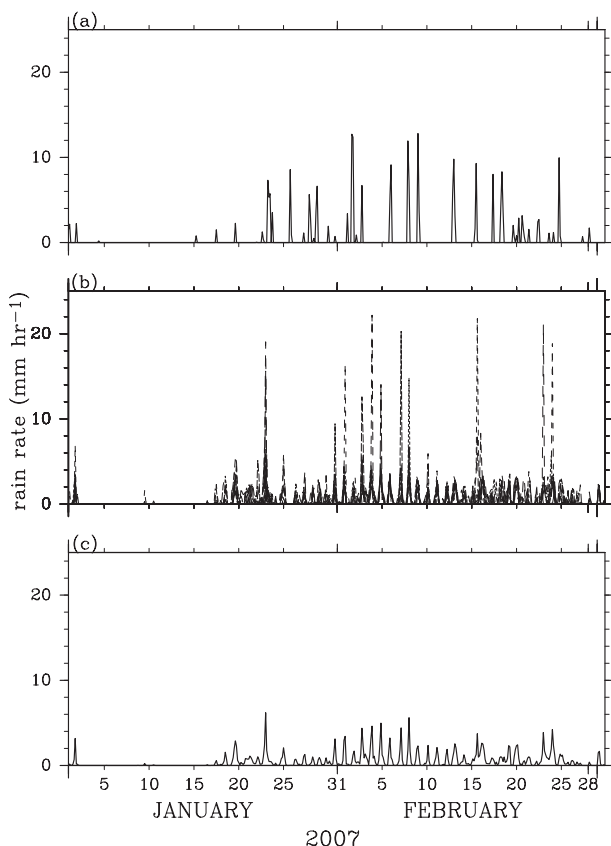
FIG. 2. (a) Time series of the TRMM estimated rainfall, (b) superimposed time series of the model-simulated precipitation rate of the nine ensemble members, and (c) time series of the ensemble mean in the unit of mm h^{-1} at the nearest grid point to the Pondok Betung Station for the 2-month period from 0000 UTC 1 Jan to 2300 UTC 1 Mar 2007. The location of Pondok Betung station is denoted by the open circle in the inset map of Fig. 1.

3. Results

a. Comparison of precipitation between the TRMM data and the model output

Figure 2 shows the time series of the TRMM estimated rainfall (Fig. 2a), the superimposed time series of the model-simulated precipitation rate of the nine ensemble members (Fig. 2b), and the time series of the ensemble mean (Fig. 2c) in mm h^{-1} at the nearest grid point to the Pondok Betung Station for the two-month period. The location of Pondok Betung is denoted by the open circle in the inset map of Fig. 1. The characteristic time scale of precipitation is generally small (less than 1 day) suggesting a convective origin, as shown by the TRMM data (Fig. 2a). The model-simulated precipitation (Fig. 2b) shows a similar time scale, which is determined by that of mesoscale convective systems. Some ensemble members show heavy precipitation (>10 mm h^{-1}) during or just after the period of the Jakarta flood event. Such

enhancement of precipitation is also discernible in the ensemble average (Fig. 2c), although the magnitude is much smaller. Both the TRMM data and the model results show modulation of the precipitation rate in the two-month period. There is little rainfall observed during the first half of January, whereas rainfall occurs frequently afterward.

Figure 3 shows the time–longitude cross sections of the TRMM-estimated rainfall data (Fig. 3a) and the ensemble mean of the model-simulated precipitation rate (Fig. 3b) averaged between 5.5° and 8°S (denoted by the two horizontal dashed lines in Fig. 1). The vertical lines in Figs. 3a,b denote the longitude of 106.6°E, which is the longitude of Pondok Betung Station. There is little rain in the first half of January in the plotted region in Fig. 3a. The dry region has a wider longitudinal extent from 60° to 140°E (not shown). After 15 January or so, rainfall increases from the western part of the domain. An enhancement of precipitation between 106° and 113°E is observed in the period of the Jakarta flood event. During the period, Jakarta is at the west end of the enhanced precipitation region and an area to the west of Jakarta remains clear. About 1 week before the flood event, the precipitation region extends from the west end of the domain to 115°E in longitude, which is wider than that in the period of the flood event. In the first half of February, precipitation is relatively limited in the plotted domain, whereas in the second half of February, precipitation increases with large longitudinal extent. It should be noted that a signal of MJO is weak for the two-month period.

The ensemble mean of the model-simulated precipitation rates (Fig. 3b) shows a good agreement with the TRMM data. The modulation of precipitation through the two-month period is well reproduced by the ensemble mean. A similar longitudinal extent of precipitation is captured in the period of the Jakarta flood event, although the model tends to show the increase of the area of weak precipitation (denoted with purple color). The model is also able to reproduce the wide area of dry condition in the first half of January and the modulation of longitudinal extent of precipitation in February.

Figure 4 shows the time–latitude cross sections of the TRMM-estimated rainfall data (Fig. 4a) and the ensemble mean of the model-simulated precipitation rate (Fig. 4b) averaged between 105.5° and 108.5°E (denoted by the two vertical dashed lines in Fig. 1). The horizontal lines in Figs. 4a,b denote the latitude of 6.2°S, which is the latitude of Pondok Betung Station in the northern part of Java. The TRMM data (Fig. 4a) show that in the first half of January, continual precipitation exists between 2° and 5°S, whereas intermittent rainfall with an interval of about 1 week exists to the north of 2°S. There is little rain to the south of 5°S during the period. The
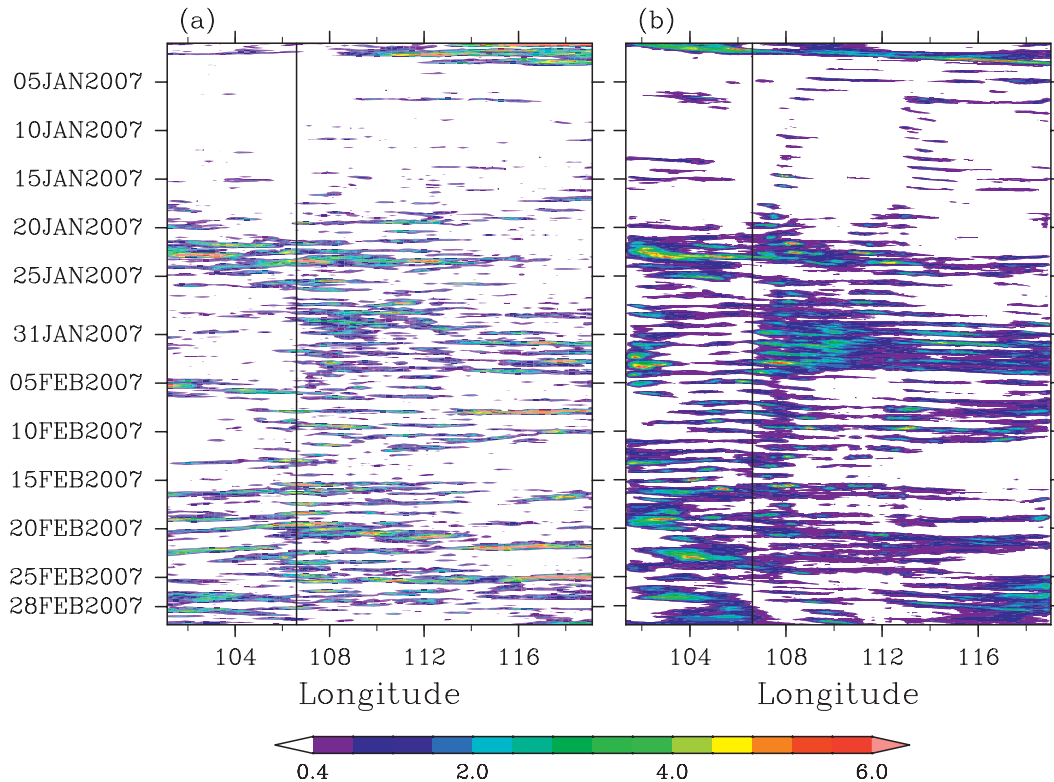
FIG. 3. Time–longitude cross sections of (a) the TRMM data and (b) the ensemble mean of the model-simulated precipitation rate averaged between 5.5° and 8°S (denoted by two horizontal dashed lines in Fig. 1). The vertical lines in (a) and (b) denote the longitude of 106.6°E, which is the longitude of Pondok Betung Station.

meridional extent of heavy rainfall occurrence varies after around 17 January. Before the Jakarta flood event, a signal of heavy rainfall propagates from 2.5°N around 25 January to 6°S around 30 January. After the signal reaches the northern part of Java, it does not propagate any farther. The meridional extent of rainfall concentrates in the latitude between 5°S and 8°S from around 30 January to 15 February. Right after 15 February, it becomes larger with a higher rain rate to the south of 6°S.

The ensemble mean of the model-simulated precipitation rates (Fig. 4b) again resembles that of the TRMM data. The north–south contrast of precipitation before around 17 January is well reproduced in the model. The propagation of a signal of heavy rainfall just before the Jakarta flood event is also well reproduced. The meridional extent of precipitation is somewhat larger in the ensemble mean from 31 January to 8 February. The modulation of intermittent precipitation to the south of 6°S in the second half of February is also well reproduced.

b. Modulation of synoptic fields

We analyze three-dimensional synoptic fields that are considered to be associated with the modulation of precipitation in the two-month period, by using the ensemble mean of the three-dimensional JMA-NHM model output. Figure 5 shows the time–latitude cross sections of the ensemble mean of the model-simulated meridional wind anomaly (Fig. 5a; m s^{-1}), temperature anomaly (Fig. 5b; °C), and relative humidity (Fig. 5c; %) at 850-hPa averaged between 105.5° and 108.5°E, which are the same as those used in Fig. 4. Here, we define an anomaly as a deviation from the two-month average.

Figure 5a shows that there is positive (northward) wind anomaly in most of the latitudes in the first 20 days of January. The propagation of a signal of negative anomaly of the meridional winds is evident from 2.5°N on 27 January to 6°S on 29 January, which corresponds to the propagation of a signal of precipitation in Fig. 4. The negative anomaly of meridional winds continues about one week at 6°S during and after the Jakarta flood event. Another event of the propagation of negative meridional wind anomaly is seen from 2.5°N on 22 January to 13°S on 24 January with some correspondence to the enhancement of precipitation shown in Fig. 4b.

A cold anomaly persists from 29 January to 4 February during and after the Jakarta flood event around 6°S (Fig. 5b). It is related to the propagation of cold anomaly, which is associated with the propagation of negative
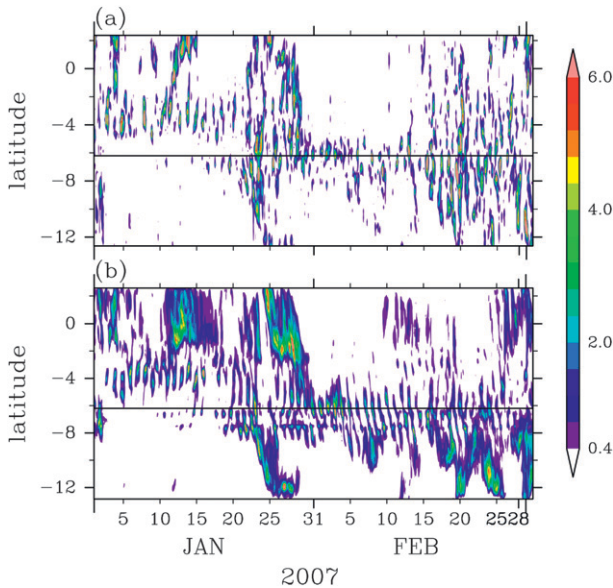
FIG. 4. Time–latitude cross sections of (a) the TRMM data and (b) the ensemble mean of the model-simulated precipitation rate averaged between 105.5° and 108.5°E (denoted by two vertical dashed lines in Fig. 1). The horizontal lines in (a) and (b) denote the latitude of 6.2°S which is the latitude of Pondok Betung Station.

anomaly of meridional wind from 27 to 29 January, as described above. The association of the cold anomaly with the northerly anomaly is indicative of a cold surge event. Continuation of the cold surge reaches 12°S on 29 January and the south end of the computational domain on 3 February. Note that there is no evidence of the cold anomaly around 22 January that corresponds to the strong negative meridional wind anomaly. This is a surge event, but not a cold surge event. Larger variability of temperature anomaly exists to the south of Java for the two-month period, in which cold (warm) anomaly dominates during January (February).

Time–latitude variations of relative humidity (Fig. 5c) shows similar pattern with those of the precipitation shown in Fig. 4b. The period of late January to early February is also marked by a moist condition near the surface (at 850 hPa) with value of relative humidity exceeding 96% over the northern part of Java. Along the horizontal line in Fig. 5 that shows the latitude of Jakarta, the temperature anomaly and relative humidity show anticorrelation, which indicates that the high humidity over Jakarta during this period is due to low temperature. This fact is confirmed by relatively low mixing ratio of water vapor during the period compared to other periods (not shown). The plot of mixing ratio also shows the airmass transformation of the cold surge that is associated with the Jakarta flood event. The air mass is dry in the Northern Hemisphere, but it gets moistened over
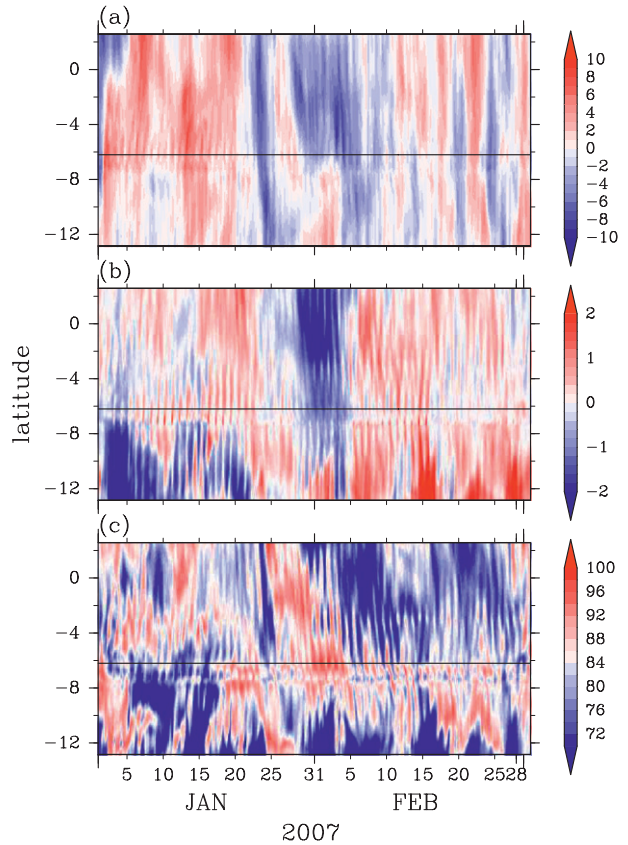

FIG. 5. As in Fig. 4, but for the ensemble mean of the model-simulated (a) meridional wind anomaly (m s^{-1}), (b) temperature anomaly (°C), and (c) relative humidity (%) at 850 hPa. We define an anomaly as a deviation from the two-month average.

the ocean, which is consistent with the description by Johnson and Houze (1987).

To see the vertical extents of the time variations described above, the time–height cross sections of the ensemble mean of the model-simulated quantities averaged over the region of West Java (5.5°–8°S, 105.5°–108.5°E) are shown in Fig. 6 for meridional wind anomaly (Fig. 6a), temperature anomaly (Fig. 6b), and relative humidity (Fig. 6c). The negative meridional wind anomaly is seen below 800 hPa from 29 January to 10 February, whereas the positive anomaly above that exists until 3 February, which constitutes the low-level vertical shear of winds as pointed out by Wu et al. (2007). During the cold anomaly period after the reach of the cold surge (29 January–4 February), the top of the cold anomaly varies from 700 to 500 hPa over West Java, whereas the top of the moist layer in which the value of relative humidity exceeds 85% varies from 600 to 800 hPa. We also note a large warm anomaly near the tropopause (above 200 hPa) during this period.

The modulation of the meridional wind anomaly near the surface shown in Fig. 5a is observed through the 2-month period, and the top of the anomaly varies from
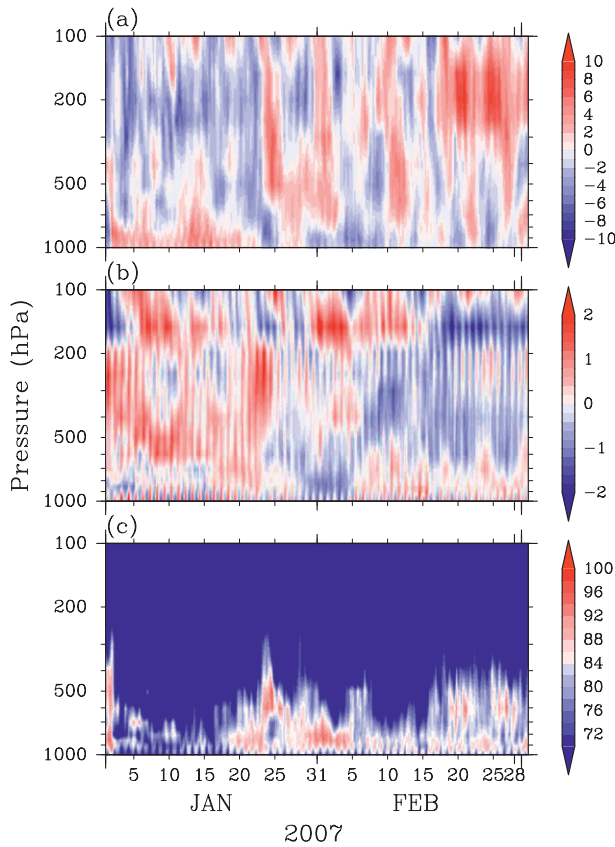
FIG. 6. Time–height cross sections of the ensemble mean of the model-simulated (a) meridional wind anomaly (m s^{-1}), (b) temperature anomaly (°C), and (c) relative humidity (%) averaged over the region of West Java (5.5°–8°S, 105.5°–108.5°E).

800 to 400 hPa. Such a modulation is also observed in the temperature anomaly, and the layer of warm anomaly near the surface becomes deeper from 17 to 20 January with the top above 200 hPa. The warm anomaly extends from the surface to 200 hPa for the following 3 days or so. During the first half of January, there is not clear moist layer near the surface. After that period, a moist layer appears near the surface, the height of which varies from about 800 to 400 hPa.

The diurnal cycle is clearly seen in the temperature anomaly through the troposphere as shown in Fig. 6b. Particularly it is strong near the surface. The diurnal cycle of relative humidity is also evident near the surface through the two-month period.

Figure 7 shows the horizontal distributions of the ensemble mean of the model-simulated precipitation rate (color; mm hr^{-1}) and horizontal winds at 850 hPa (arrows; m s^{-1}) averaged for each pentad. Here, we only show 6 pentads, pentads 3–8, including pentad 7 (31 January–4 February) in which the heavy rainfall event occurred in Jakarta. In pentad 7, a zonally elongated rainband is formed around 5°–6°S, 106°–119°E. In that

period, Jakarta is located at the western edge of the rainband as already noticed in Fig. 3. There is small amount of rainfall to the north and south of the rainband. The rainband in pentad 7 is consistent with the increase of convergence of horizontal winds at 850 hPa (not shown).

A cold surge is captured through pentads 5–7. In pentad 5, a typical Borneo vortex appears; the northeasterly winds over the South China Sea change their direction to southeastward over and around Sumatra, and the wind is roughly eastward over West Java. In pentad 6, the eastern part of the vortex disappears, and further deformation of the vortex continues. In pentad 7, the winds over the South China Sea become almost northerly. The wind speed increases near West Java and the northerly component increases from pentad 6 to pentad 7. The northerly component of the surface wind intensifies upward motion on the northern slope of the mountain range in West Java. The surge event terminates in pentad 8.

In association with the modulation of the horizontal wind field, the horizontal distribution of heavy precipitation changes from pentad to pentad. In pentad 5, weak precipitation less than 1 mm h^{-1} covers the middle and northern parts of the computational domain with some intensification over the South China Sea. In pentad 6, heavy precipitation areas appear over the South China Sea and the Java Sea. In pentad 7, the heavy precipitation area over the South China Sea disappears, while that over the Java Sea moves southward to form the zonally elongated rainband. The rainband disappears in pentad 8.

c. Three-dimensional structures of the Borneo vortex and the cold surge

Figure 8 shows the latitude–height cross sections of the ensemble mean of the model-simulated temperature anomaly from the two-month average (color; °C), and meridional and vertical winds (arrows; m s^{-1}) averaged between 105.5° and 108.5°E for each pentad. In pentad 7 (Fig. 8e), in which heavy rainfall occurred at Jakarta, southward flow covers to the north of 7°S below the 800-hPa level. Large upward motion can be seen from the surface to 250 hPa over the convergence region of horizontal winds around 6°S near the front of the southward flow. The southward flow is associated with a cold anomaly as previously shown in Figs. 5b and 6b, which is clearer below the 850-hPa level. The large warm anomaly near the tropopause noted in Fig. 6b has the maximum just above the area of the large upward motion with a meridional extent of about 5°. In pentad 5 (Fig. 8c), on the other hand, the southward flow below the 700-hPa level is mostly warm. Near the center of the Borneo vortex (2°S), upward motion dominates throughout the troposphere with a warm anomaly centered at around 250 hPa. In pentad 3 (Fig. 8a), a similar upward
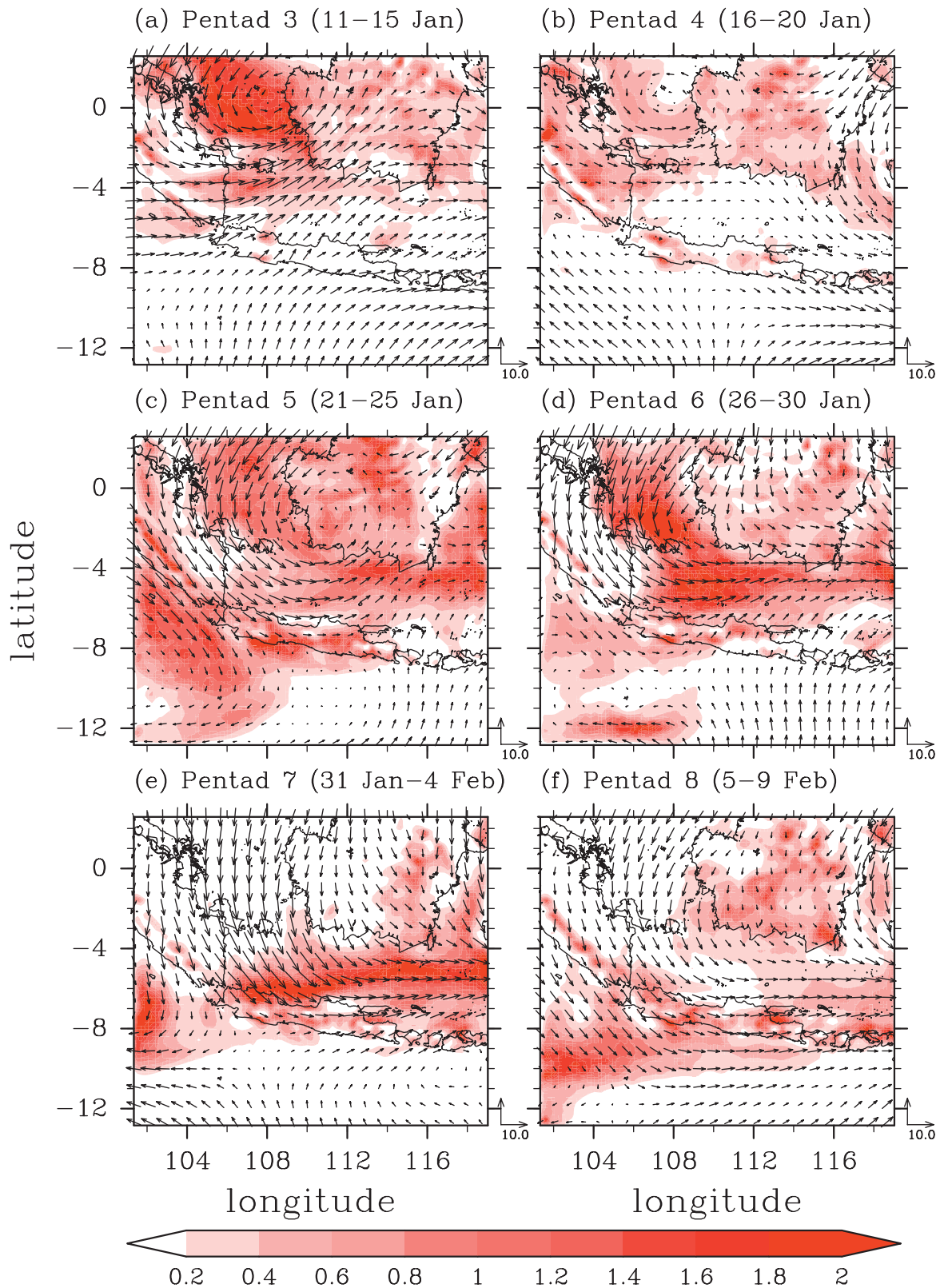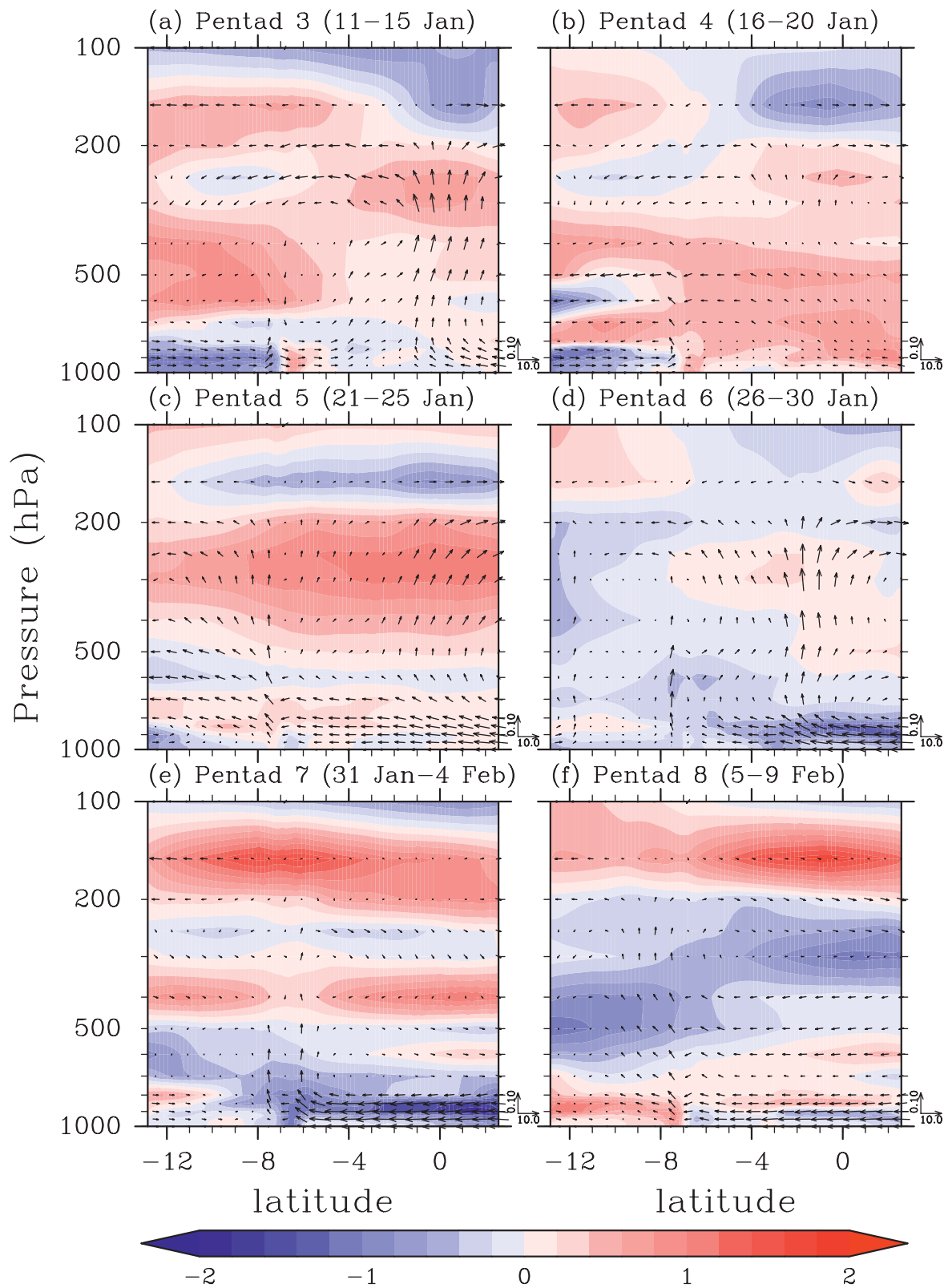
(a) Pentad 3 (11−15 Jan)

(b) Pentad 4 (16−20 Jan)

(c) Pentad 5 (21−25 Jan)

(d) Pentad 6 (26−30 Jan)

(e) Pentad 7 (31 Jan−4 Feb)

(f) Pentad 8 (5−9 Feb)

FIG. 7. Horizontal distributions of the ensemble mean of the model-simulated precipitation rate (color; mm h^{-1}) and horizontal winds (arrows; m s^{-1}) at 850 hPa averaged for each pentad. Unit vectors (10 m s^{-1}, 10 m s^{-1}) are shown on the bottom-right corner in each plot.

FIG. 8. Latitude–height cross sections of the ensemble mean of the model-simulated temperature anomaly from the two-month average (color; °C), and meridional and vertical winds (arrows; m s^{-1}) averaged between 105.5° and 108.5°E for each pentad. Unit vectors (10 m s^{-1}, 0.1 m s^{-1}) are shown on the bottom-right corner in each plot.

motion with a warm anomaly at around 250 hPa is also observed near the center of the Borneo vortex (equator). From pentads 5–7, the southward flow near the surface becomes colder and shallower; in pentad 5, the top of the southward flow is at 600 hPa, whereas in pentads 6 and 7, the top of the southward flow becomes 800 hPa. Note that in every pentad the upward motion exists at 7.5°S, which corresponds to the southern coast of Java.

Figure 9 shows the horizontal distributions of the ensemble mean of the model-simulated vertical winds (color; m s^{-1}) and horizontal winds (arrows; m s^{-1}) for pentad 5 (21–25 January) at (Fig. 9a) 300, (Fig. 9b) 500, (Fig. 9c) 700, and (Fig. 9d) 925 hPa, as well as (Fig. 9e) the ensemble mean of the model-simulated precipitation rate (color; mm h^{-1}) and horizontal winds (arrows; m s^{-1}) at the surface, and (Fig. 9f) the TRMM precipitation rate (color; mm h^{-1}) and QuikSCAT sea surface winds (arrows; m s^{-1}). The Borneo vortex is clearly identified from the surface to 700 hPa, whereas its appearance is not noticeable at 500 hPa. At 300 hPa, the wind direction is almost westward over the vortex. From the surface to 700 hPa, the center of the Borneo vortex shifts to the southwestward with height toward the southern South China Sea: (0°, 112°E) at 925 hPa (Fig. 9d), (1°S, 111°E) at 850 hPa (Fig. 7c), and (2°S, 110°E) at 700 hPa (Fig. 9c). Upward motion is dominant over the central part of Borneo and the areas to the west and south of the island from 925 up to 300 hPa (Figs. 9a–d; see also Fig. 8c for the meridional cross section). The areas of large upward motion, including those to the south of Sumatra and Java, correspond well to the areas where precipitation in the model becomes large (Fig. 9e). The horizontal distribution of vertical winds shows the similar pattern through the troposphere with larger magnitude in the upper troposphere. Note that the small-scale pattern of the vertical winds over the islands seems to represent stationary gravity waves over mountainous regions.

The surface winds from QuikSCAT (Fig. 9f) show a good agreement with the model-simulated surface winds (Fig. 9e). Southward winds blow over the South China Sea, and turn eastward over the Java Sea. On the other hand, northward winds blow to the south of Java. The distribution of precipitation in the model (Fig. 9e) is also in good agreement with that of the TRMM observation (Fig. 9f); precipitation is higher in the areas to the west and south of Borneo, and to the south of Sumatra and Java. Note that the pattern of precipitation in the observation (Fig. 9f) shows aggregates of spots, whereas that of the model simulation (Fig. 9e) shows a smooth distribution as a result of the ensemble mean. The ensemble mean pattern represents a probability of the occurrence of precipitation, whereas each member of the ensembles shows aggregates of spots due to the distribution of rather isolated convective systems.

Figure 10 shows the same horizontal distributions as Fig. 9 but for pentad 7. Strong southward flow of the cold surge as shown in Fig. 8e is clearly seen from the surface (Fig. 10e) to 850 hPa (Fig. 7e), but it disappears at 700 hPa (Fig. 10c). Convergence of the horizontal winds associated with the cold surge and its continuation over the Java Sea produces large upward motions along the zonal band to the north of Java around 5°–6°S and 106°–119°E through the troposphere (Figs. 10a–d). At 500 and 300 hPa, horizontal winds show divergence over the zonal band that corresponds to the band of heavy precipitation (Fig. 10e). Downward motion prevails outside the zonal band through the troposphere and little precipitation is observed there. The comparison of the surface winds between the model output and QuikSCAT also shows a good agreement in pentad 7.

d. Modulation of the statistics on precipitation rate

We use frequency distribution functions of ensemble simulation data to investigate the modulation of the statistics on the precipitation rate on the time scale of pentads. The cumulative distribution function (CDF) of the model-simulated precipitation rate for each pentad is computed using grids in the land region of West Java (the hatched area in the inset map in Fig. 1) in the course of 5 days for the 9 ensemble members. When computing the CDF, we exclude grids without precipitation to avoid high probabilities for the bin of no precipitation in the histograms. Figure 11 shows the CDF only for the upper tail of the distribution (94%–100%) for each pentad as we focus on the heavy rainfall part. The fraction of grids with precipitation is also included in each panel, which is defined for each pentad as follows:

$$\mathrm{fr} = \frac{\text{non-zero precipitation sample size}}{\text{total sample size}} \times 100\%. \quad (1)$$

For the first 3 pentads, the value of fr is less than 16%, whereas the highest value is about 48% for pentad 7 and the second highest value is about 38% for pentad 11.

The probabilistic modulation of precipitation is apparent in the CDFs. In the first three pentads, the fraction of heavy rainfall is smaller than that for the whole period denoted by the dashed curve, whereas in pentads 5, 7, and 10, the fraction of heavy rainfall is greater than that for the whole period. To quantify the modulation, we introduce a threshold value of 10 mm h^{-1} for the heavy rainfall events (the vertical dashed line in each panel). In pentads 1–3, the contribution of the heavy rainfall is less than 1.2%, whereas those in pentads 5, 7, and 10 are 4.0%, 3.3%, and 3%, respectively. These numbers are
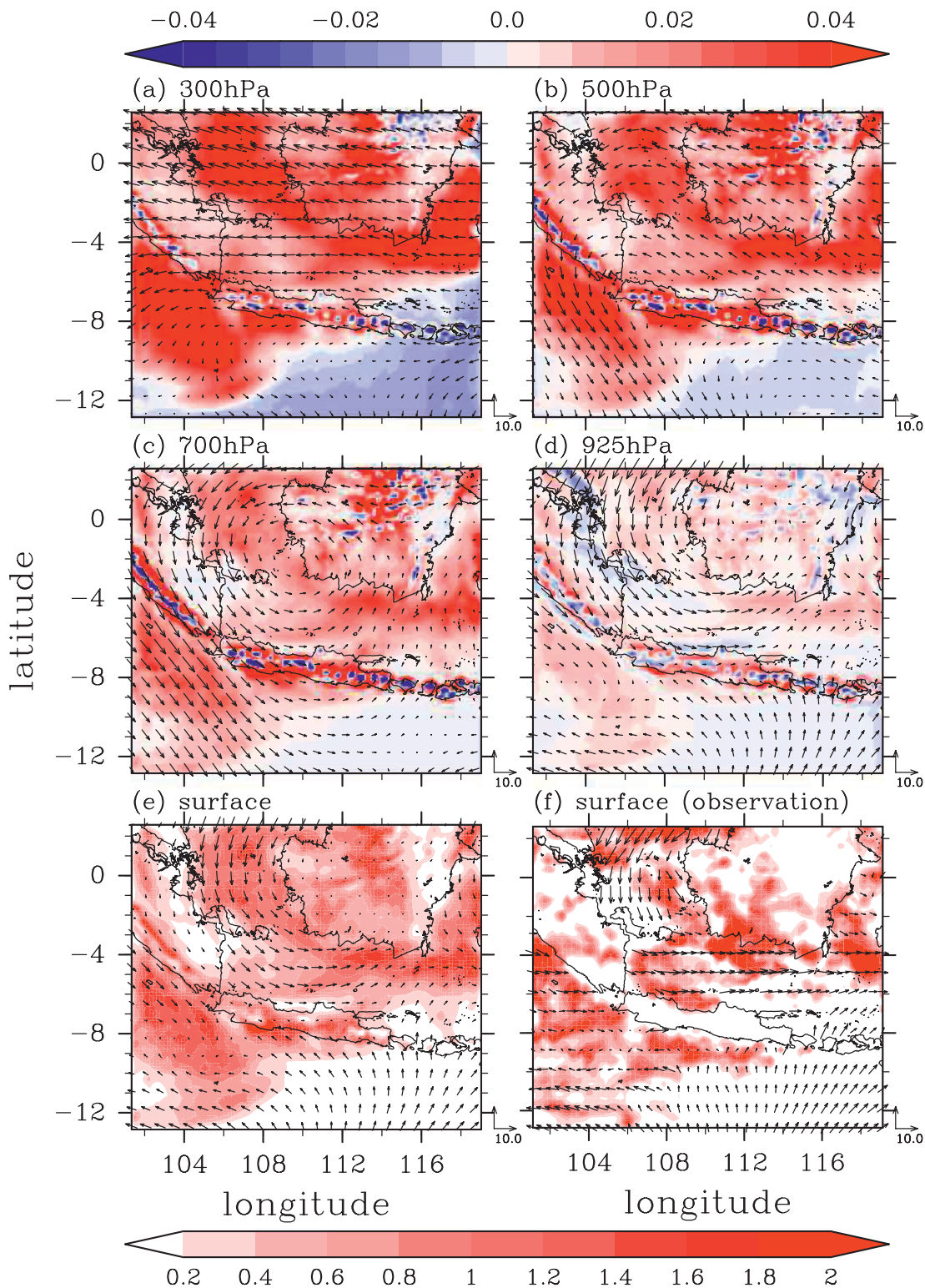
FIG. 9. Horizontal distributions of the ensemble mean of the model-simulated vertical winds (color) and horizontal winds (arrows) for pentad 5 (21–25 Jan) at (a) 300, (b) 500, (c) 700, and (d) 925 hPa. Horizontal distributions of (e) the ensemble mean of the model-simulated precipitation rate and horizontal winds at the surface, and (f) the TRMM precipitation rate and QuikSCAT sea surface wind. The top color bar in the unit of m s^{-1} is for (a)–(d) and the bottom one in the unit of mm h^{-1} is for (e),(f). Unit vectors (10 m s^{-1}, 10 m s^{-1}) are shown on the bottom-right corner in each plot.
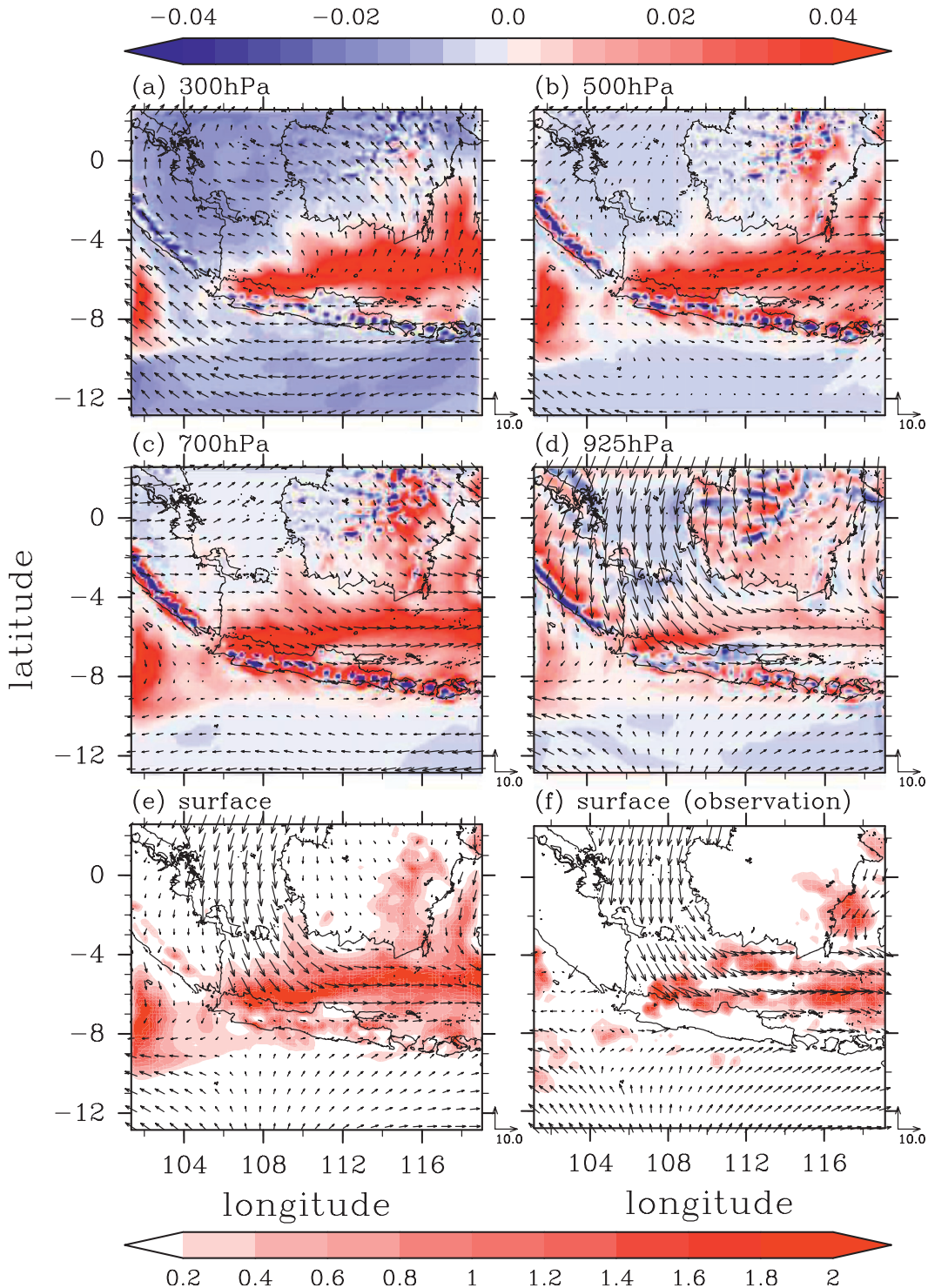
FIG. 10. As in Fig. 9, but for pentad 7 (31 Jan–4 Feb 2007).

about a factor of 3 or more compared to the minimum value during the 2-month period.

To find out local time dependence of the heavy rainfalls, Fig. 12 shows the diurnal variation of heavy rainfall occurrence over the land region of West Java (solid lines) and over the Java Sea (dashed lines; the box with a horizontal hatch pattern in Fig. 1) in each pentad. Three different values of rain rate, 10, 20, and 30 mm h^{-1}, are
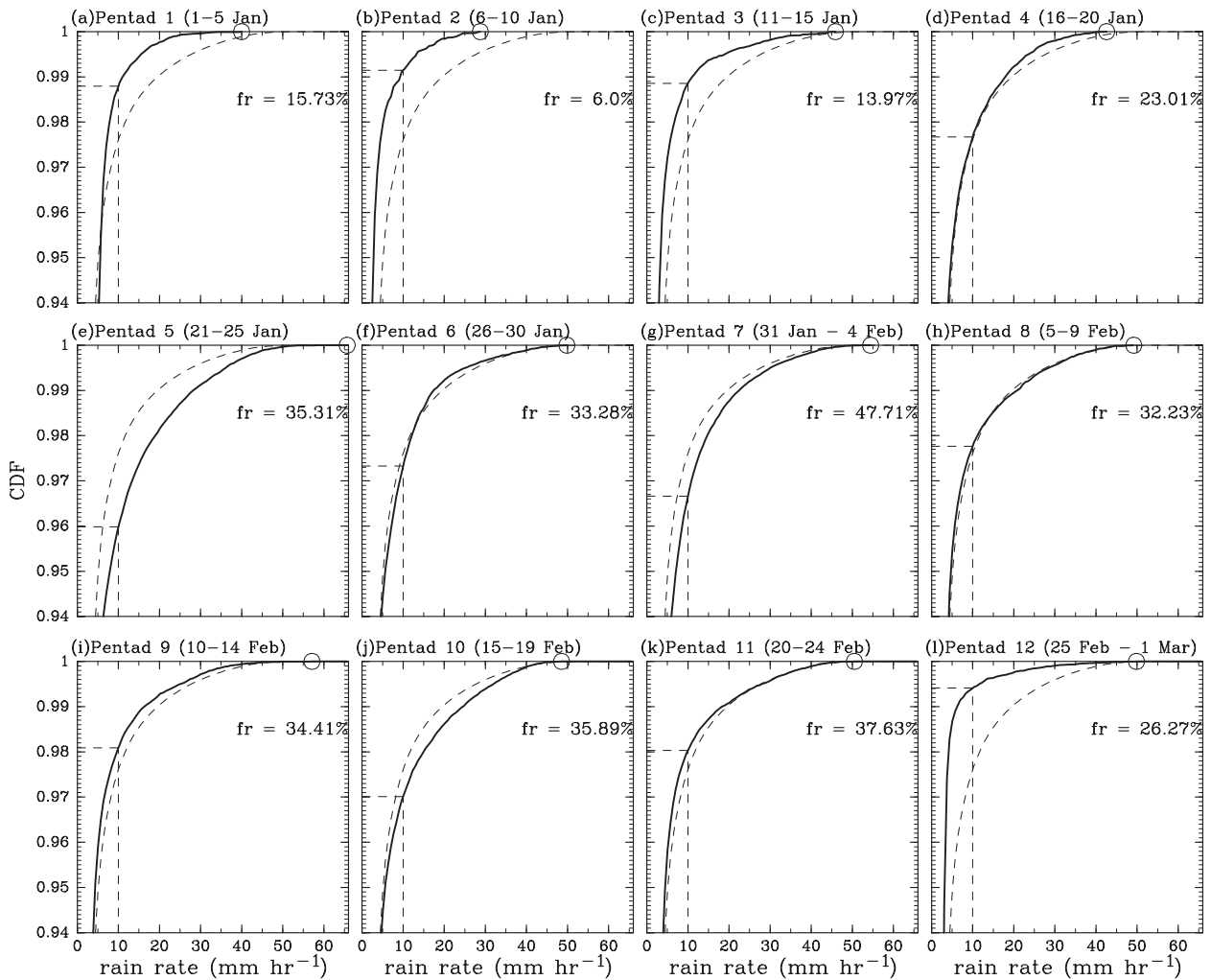
FIG. 11. Cumulative distribution function of the model-simulated precipitation rate for (top left to bottom right) pentads 1–12 computed from all the ensemble members for grids in the land region of West Java. The dashed curve is the CDF for the two-month period. The circle denotes the highest value of rain rate in each pentad. The vertical and horizontal dashed lines show the intersection point of the 10 mm h^{-1} rain rate and its cumulative probability value. The value fr is defined by Eq. (1).

selected as a threshold value to define a heavy rainfall event, but we obtain a robust result that is not sensitive to the choice of the threshold value. As already seen in Fig. 11, heavy rainfall events over the land are frequently identified in pentads 5, 7, and 10, during which semi-diurnal variations are dominant. That is, two peaks of the occurrence are clearly seen in these pentads. In pentad 7, the largest peak appears at 0500–0600 LT (LT denotes local time at Jakarta) and the second peak appears at 2200 LT. In pentad 5, there are two peaks in the morning and in the evening with similar numbers of grids, while the largest peak appears in the late evening and the second peak appears in the morning in pentad 10.

The maximum of heavy rainfall occurrence over the ocean appears in the morning in all pentads (dashed lines). Unlike over the land, the largest peak over the

ocean appears in pentad 6, which is consistent with the southward movement of the rainband from pentads 6–7 as shown in Figs. 7d–e. The second largest peak over the ocean appears in pentad 3, which is the period of a Borneo vortex event. In pentad 7, during which the Jakarta flood event occurred, there are three peaks: 0200, 0700, and 1400 LT.

4. Discussion

Cold surges have been studied for decades. Previous studies focused on large-scale features on time scales of submonthly to seasonal (e.g., Compo et al. 1999; Chang et al. 2005), or small-scale features on time scales of several days, including case studies (e.g., Wu et al. 2007; Tangang et al. 2008) and composite analyses (e.g., Compo et al.
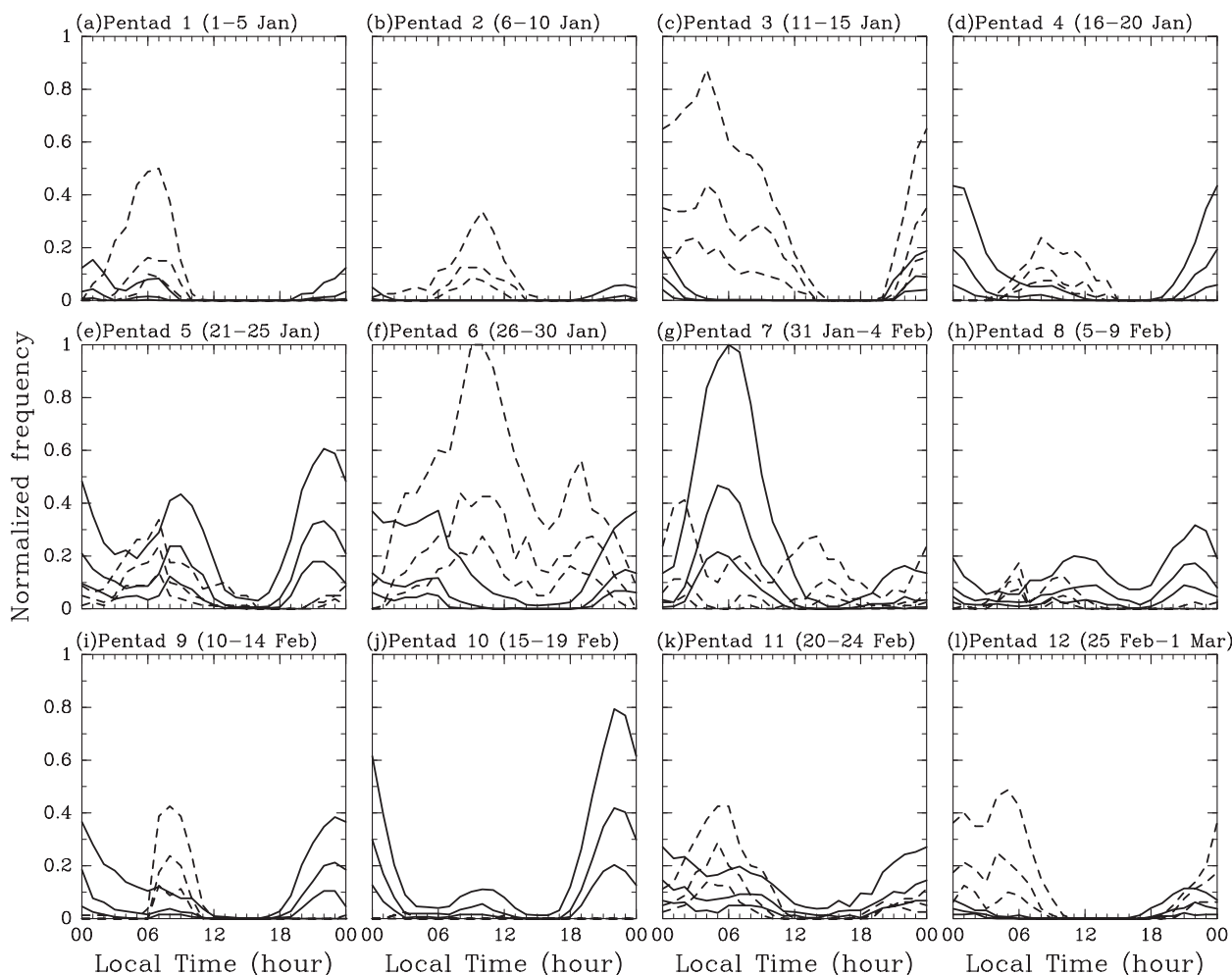
FIG. 12. Diurnal variation of heavy rainfall occurrence in (top left to bottom right) pentads 1–12 over the land region of West Java (solid lines) and over the Java Sea (dashed lines) as illustrated in Fig. 1. The top, middle, and bottom lines for each region denote the normalized frequency of rain rate exceeding 10, 20, and 30 mm h^{-1}, respectively. The frequency is normalized by the maximum value for 10 mm h^{-1} for each region (325 grids in pentad 7 out of 6300 grids for land and 80 grids in pentad 6 out of 8145 grids for ocean).

1999). In contrast, this paper investigates the modulation of heavy precipitation and related three-dimensional structures due to cross-equatorial monsoon surges around Southeast Asia on the time scales from less than one day to two months. It is confirmed that changes in the vertical profiles of moist thermodynamic conditions during the Jakarta flood event obtained by radiosonde observations (Wu et al. 2007) are associated with the three-dimensional synoptic field related to the cross-equatorial cold surge event that reached Java. Our model output gives the top of cold northerly as 1.5 km, or equivalently 850 hPa. This cold surge event is preceded by the Borneo vortex event as shown in Figs. 7c, 8c, and 9.

The Borneo vortex is centered at (1°S, 111°E) at 850 hPa in pentad 5, in which precipitation over West Java is relatively weak. Another Borneo vortex event is also captured by the model in pentad 3 (11–15 January,

Fig. 7a), when the heavy precipitation occurred in the southern tip of Malay Peninsula, which faces the South China Sea, as reported by Tangang et al. (2008). Strong convergence associated with a northeasterly cold surge exists over a tip of Malay Peninsula during the event. Although Tangang et al. (2008) argued that this was not a vortex event based on reanalysis data with the 2.5° × 2.5° resolution, our model output with the 20-km resolution shows the existence of the vortex.

The shift of the center of the Borneo vortex with height as seen in Fig. 9 has a horizontal displacement of about 100 km, whereas the horizontal scale of the vortex is about 1000 km. This kind of slantwise structure with a similar geometry in the tropics is also reported by Otsuka and Yoden (2005), although they focused on a displacement of not a vortex center but a saddle point between two synoptic-scale vortices. Weakness of geostrophic constraint

near the equator may allow these slantwise structures within thin layers.

On the other hand, the vortex disappears in pentad 7, during which the heavy rainfall occurred at Jakarta. This is consistent with the fact reported by Chang et al. (2005) that the regions to the south of the South China Sea (namely the Java Sea) experience enhanced convection when the Borneo vortex is absent.

In pentad 7, more frequent occurrence of heavy precipitation is observed compared to other periods in the time series of precipitation for nine ensemble members as shown in Fig. 2b. For this ensemble experiment, well-sampled probability distributions are obtained by using the grids in the land region of West Java in the course of 5 days for all the ensemble members as shown in Fig. 11. The ensemble experiment with a relatively low-resolution model with a cumulus parameterization allowed us to capture the enhancement of localized heavy precipitation in pentad 7 compared to other pentads. On the other hand, a high-resolution experiment for the same period with only one member would be hard to obtain such statistics with the same computational resources; this is a trade-off. Note that the CDFs in Fig. 11 are normalized by the number of the grids with precipitation, so that the actual number of the grids with heavy precipitation is proportional to the value of fr times the value of the corresponding CDF.

As shown in Fig. 12, diurnal variation of heavy precipitation over the land usually has a peak in the late evening, whereas that over the ocean has a peak in the morning, which is consistent with the geographical distribution of the diurnal variation of precipitation estimated from satellite observations (e.g., Mori et al. 2004; Hirose and Nakamura 2005). Semidiurnal variation of heavy precipitation in some pentads implies that the coastal region of West Java is affected by convective systems of both over the land and ocean. In pentad 7 (Fig. 12g), the highest peak of the occurrence of heavy rainfall over the ocean appears at 0200 LT, whereas that over the land appears around 0500–0600 LT. This time lag suggests that the convective systems are initiated over the ocean, move southward, and intensify over the land region. A similar time lag of the morning rain can also be seen in pentads 5 and 8, in which the semidiurnal variation is seen over the land. In such pentads, the morning rain over the ocean plays an important role to produce the semidiurnal variation over the land.

5. Conclusions

A time-lagged ensemble simulation using a regional numerical model is employed to investigate the modulation of precipitation over West Java in the two-month period of January–February 2007. Comparison between the numerical results and the TRMM 3B42 data shows a fundamental agreement on the temporal modulation of the spatial distributions of precipitation as shown in Figs. 2, 3, and 4 including the enhancement of precipitation on the time scale of pentads during the period of heavy rainfall, from 31 January to 4 February, during the Jakarta flood event. Comparison between the surface winds in the model and those of QuikSCAT also shows good agreement as shown in Figs. 9e,f and 10e,f.

In addition to the modulation of meridional winds reported by Wu et al. (2007), modulation of temperature and relative humidity is also investigated with the time–latitude cross sections (Fig. 5) and the time–height cross sections (Fig. 6). During the two-month period, several monsoon surges are observed, among which only the surge event during the Jakarta flood event is associated with the cold anomaly. The event is preceded by the Borneo vortex event in pentad 5 shown in Figs. 7c and 9. We have investigated the pentad-to-pentad modulation of synoptic fields and precipitation, and found that only pentad 7, which includes the Jakarta flood event, has the zonal band of heavy precipitation to the north of Java (Figs. 7e and 10e).

Further investigation on the vertical distributions of meridional and vertical winds and temperature anomaly (Fig. 8) indicates that the southward flow near the surface is getting colder and shallower from the period of Borneo vortex event (pentad 5) to the period of the cold surge event (pentads 6 and 7). The top of the cold northerly during the Jakarta flood event is about 1.5 km (850 hPa). The Borneo vortex in pentad 5 is clear from the surface to 700 hPa as shown in Figs. 8c and 9c. The vortex has a slantwise structure within such a thin layer under weak constraint of geostrophy near the equator.

A statistical analysis with a cumulative distribution function is employed to investigate the modulation of the probability of rainfall rate based on the samples over the land region of West Java with all ensemble members for each pentad. It is found that in pentad 7 the fraction of rain is highest for the two-month period as shown in Fig. 11g. Pentad 7 also marks one of the highest values for the contribution of heavy precipitation, which is about 3 times larger than the minimum value during the 2-month period. This is indicative of the possibility of using this kind of quantity for the potential forecast of heavy precipitation in the future as a product of ensemble forecasts. The diurnal cycle of occurrence of heavy rainfall is also modulated during the two-month period; in pentad 7, semidiurnal variation becomes dominant, and the largest peak appears in the early morning.

REFERENCES

Branković, Č., T. N. Palmer, F. Molteni, S. Tibaldi, and U. Cubasch, 1990: Extended-range predictions with ECMWF models: Time-lagged ensemble forecasting. *Quart. J. Roy. Meteor. Soc.,* **116,** 867–912.

Chang, C.-P., P. A. Harr, and H.-J. Chen, 2005: Synoptic disturbances over the equatorial South China Sea and western Maritime Continent during boreal winter. *Mon. Wea. Rev.,* **133,** 489–503.

Cheang, B. K., 1977: Synoptic features and structures of some equatorial vortices over the South China Sea in the Malaysian region during the winter monsoon of December 1973. *Pure Appl. Geophys.,* **115,** 1303–1333.

Chelton, D. B., and M. H. Freilich, 2005: Scatterometer-based assessment of 10-m wind analyses from the operational ECMWF and NCEP numerical weather prediction models. *Mon. Wea. Rev.,* **133,** 409–429.

Compo, G. P., G. N. Kiladis, and P. J. Webster, 1999: The horizontal and vertical structure of east Asian winter monsoon pressure surges. *Quart. J. Roy. Meteor. Soc.,* **125,** 29–54.

Freilich, M. H., and R. S. Dunbar, 1999: The accuracy of the NSCAT 1 vector winds: Comparisons with National Data Buoy Center buoys. *J. Geophys. Res.,* **104,** 11 231–11 246.

Hayashi, S., K. Aranami, and K. Saito, 2008: Statistical verification of short term NWP by NHM and WRF-ARW with 20 km horizontal resolution around Japan and Southeast Asia. *SOLA,* **4,** 133–136.

Hirose, M., and K. Nakamura, 2005: Spatial and diurnal variation of precipitation systems over Asia observed by the TRMM Precipitation Radar. *J. Geophys. Res.,* **110,** D05106, doi:10.1029/2004JD004815.

Huffman, G. J., and Coauthors, 2007: The TRMM Multisatellite Precipitation Analysis (TMPA): Quasi-global, multiyear, combined-sensor precipitation estimates at fine scales. *J. Hydrometeor.,* **8,** 38–55.

Johnson, R. H., and R. A. Houze Jr., 1987: Precipitating cloud systems of the Asian monsoon. *Monsoon Meteorology,* C.-P. Chang and T. N. Krishnamurti, Eds., Oxford University Press, 298–353.

Juneng, L., F. T. Tangang, and C. J. C. Reason, 2007: Numerical case study of an extreme rainfall event during 9–11 December 2004 over the east coast Peninsular Malaysia. *Meteor. Atmos. Phys.,* **98,** 81–98.

Mittermaier, M. P., 2007: Improving short-range high-resolution model precipitation forecast skill using time-lagged ensembles. *Quart. J. Roy. Meteor. Soc.,* **133,** 1487–1500.

Mori, S., and Coauthors, 2004: Diurnal land–sea rainfall peak migration over Sumatera Island, Indonesian Maritime Continent, observed by TRMM satellite and intensive rawinsonde soundings. *Mon. Wea. Rev.,* **132,** 2021–2039.

Nakanishi, M., and H. Niino, 2004: An improved Mellor-Yamada level 3 model with condensation physics: Its design and verification. *Bound.-Layer Meteor.,* **112,** 1–31.

——, and ——, 2006: An improved Mellor-Yamada level-3 model: Its numerical stability and application to a regional prediction of advection fog. *Bound.-Layer Meteor.,* **119,** 397–407.

Otsuka, S., and S. Yoden, 2005: Numerical experiments on the layered structures in the mid-troposphere over the equatorial Pacific. *SOLA,* **1,** 69–72.

Saito, K., and Coauthors, 2006: The operational JMA nonhydrostatic mesoscale model. *Mon. Wea. Rev.,* **134,** 1266–1298.

——, J. Ishida, K. Aranami, T. Hara, T. Segawa, M. Narita, and Y. Honda, 2007: Nonhydrostatic atmospheric models and operational development at JMA. *J. Meteor. Soc. Japan,* **85B,** 271–304.

Seko, H., S. Hayashi, M. Kunii, and K. Saito, 2008: Structure of the regional heavy rainfall system that occurred in Mumbai, India, on 26 July 2005. *SOLA,* **4,** 129–132.

Suppiah, R., and X. Wu, 1998: Surges, cross-equatorial flows and their links with the Australian summer monsoon circulation and rainfall. *Aust. Meteor. Mag.,* **47,** 113–130.

Tangang, F. T., L. Juneng, E. Salimun, P. N. Vinayachandran, Y. K. Seng, C. J. C. Reason, S. K. Behera, and T. Yasunari, 2008: On the roles of the northeast cold surge, the Borneo vortex, the Madden-Julian Oscillation, and the Indian Ocean Dipole during the extreme 2006/2007 flood in southern Peninsular Malaysia. *Geophys. Res. Lett.,* **35,** L14S07, doi:10.1029/2008GL033429.

Wangwongchai, A., S. Zhao, and Q. Zeng, 2005: A case study on a strong tropical disturbance and record heavy rainfall in Hat Yai, Thailand during winter monsoon. *Adv. Atmos. Sci.,* **20,** 436–450.

Wu, P., M. Hara, H. Fudeyasu, M. D. Yamanaka, J. Matsumoto, F. Syamsudin, R. Sulistyowati, and Y. S. Djajadihardja, 2007: The impact of trans-equatorial monsoon flow on the formation of repeated torrential rains over Java Island. *SOLA,* **3,** 93–96.

Yabu, S., S. Murai, and H. Kitagawa, 2005: Clear-sky radiation scheme (in Japanese). NPD Rep., Vol. 51, Numerical Prediction Division, JMA, 53–64.

Yoden, S., 2007: Atmospheric predictability. *J. Meteor. Soc. Japan,* **85B,** 77–102.